Experimental demonstration of nonuniform frequency distributions of granular packings

Guo-Jie Gao,[1] Jerzy Blawzdziewicz,[1,2] Corey S. O'Hern,[1,2] and Mark Shattuck[3]
[1]*Department of Mechanical Engineering, Yale University, New Haven, Connecticut 06520-8286, USA*
[2]*Department of Physics, Yale University, New Haven, Connecticut 06520-8120, USA*
[3]*Benjamin Levich Institute and Physics Department, The City College of the City University of New York, New York, New York 10031, USA*

(Received 28 March 2009; revised manuscript received 3 September 2009; published 17 December 2009)

We developed an experimental method to generate mechanically stable (MS) packings of *frictionless* disks and performed coordinated experiments and simulations to characterize MS packings in small systems. For a given system geometry, MS packings occur as discrete, well-separated points in configuration space with probabilities that vary by many orders of magnitude and are robust with respect to the packing preparation. Over a continuous range of system geometries, MS packings occur as distinct geometrical families and only a small fraction of families are sampled via quasistatic dynamics. These results suggest that the most frequent MS packings may dominate the structural and mechanical properties of dense granular media.

DOI: 10.1103/PhysRevE.80.061304 PACS number(s): 83.80.Fg, 61.43.−j, 05.20.−y, 64.70.kj

Equilibrium statistical mechanics provides a powerful method to determine the macroscopic state of thermal systems by counting the number of microstates. Several recent studies have applied similar methods to describe dense granular materials [1–4]. Many of these have used Edwards-ensemble descriptions, which are based on an assumption that all static configurations of a granular system under a given set of macroscopic constraints are equally likely [5].

Despite the fact that granular media are dissipative and require external driving forces (not thermal fluctuations) to explore configuration space, there has been surprising success in describing static and slowly evolving granular systems using statistical methods based on the Edwards' assumption [6–9]. However, the assumption of equal microstate probability has not been tested explicitly and the relevant microstates have not been clearly defined. We advocate a "bottom-up" approach to constructing statistical-mechanics descriptions of dense granular materials—one where we enumerate the microstates and accurately measure their probabilities [10,11].

To study microstate statistics, we performed experiments and simulations of static packings in two dimensions (2D). We focused on small frictionless systems to enable enumeration of nearly all mechanically stable (MS) packings (i.e., microstates). Frictionless MS disk packings possess two important characteristics: (1) force balance is achieved on all grains and (2) all possible single and collective particle displacements (except those arising from rattler particles) lead to particle overlaps and increases in energy [10]. In experiments, an ensemble of packings is obtained by randomizing the system using large-amplitude vibrations and in simulations packings are generated using deposition under gravity from random initial positions. To generate *frictionless* packings in experiments, we developed a technique where frictional forces are relaxed using small-amplitude, high-frequency vibrations. This method allows one to differentiate the effects of geometrical constraints from friction and thus it has broad applicability.

We find the following four key results concerning microstate distributions for frictionless MS packings: (1) The sets of MS packings found in experiments and simulations are nearly identical. (2) For a specific system geometry, there is a finite number of discrete MS packings. These packings possess highly *nonuniform* frequencies (contrary to the Edwards' hypothesis) that are relatively insensitive to packing preparation. (3) Over a continuous range of system geometries, MS packings can be classified using a finite number of geometrical families characterized by the particle contact network. (4) During uniaxial quasistatic compression, the system samples a small fraction of families. The fraction decreases with increasing strain, which indicates highly *nonergodic* evolution.

The apparatus for generating frictionless disk packings is depicted in Fig. 1. A mixture of thin disks with two different diameters (diameter ratio $d=\sigma_l/\sigma_s=1.252$) was confined between two glass plates. The cell rests on a thin plunger and is connected to an electromagnetic shaker through a slot in the

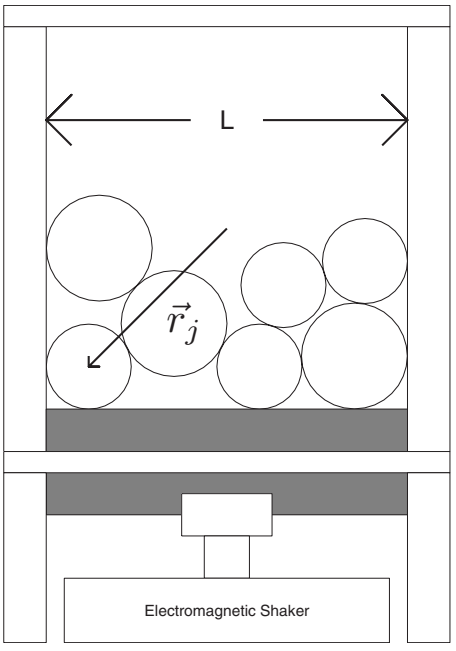

FIG. 1. Schematic of the experiment used to generate mechanically stable frictionless granular packings.

bottom. The shaker enabled us to apply vertical vibrations at variable amplitude and frequency to repeatedly generate MS packings. The mixtures consisted of an odd number of grains ($N=5$ and 7) with one more small than large disk. The separation L between the side walls can vary from zero to $6\sigma_s$ by fixing one wall and moving the other via a stepper motor. A force transducer measures the applied force.

We employed two experimental procedures to study MS packings: (a) enumeration of nearly all packings at fixed cell width L and (b) quasistatic changes in L to study dynamics from one MS packing to another. To generate an ensemble of packings at a given width, we first oscillated at high amplitude and low frequency (50 Hz) for at least 1 s to randomize particle positions and then relaxed the system under gravity with the shaker turned off for 400 ms. We applied a low-amplitude, high-frequency (400 Hz) oscillation for 500 ms, which excites particle rotation and relaxes frictional forces. Finally, oscillations were turned off and particles came to rest. Particle positions were captured to an accuracy of $\Delta/\sigma_s=6\times10^{-6}$. The MS packings were classified using the set of particle positions $\vec{R}_i=\{\vec{r}_1,\vec{r}_2,\ldots,\vec{r}_N\}$ for configuration i, where $\vec{r}_j$ gives the coordinates of the N particles.

For quasistatic dynamics, we initialized the system in one of the MS packings at large wall separation $L_{\max}/\sigma_s=1+4\sqrt{d}$. We compressed the system by successively decreasing L in 100 small increments. During each step, we applied low-amplitude, high-frequency oscillations to remove friction. If the applied force F was greater than a large threshold F_t, the shaking amplitude was increased and frequency decreased until $F<F_t$. We compressed the system to $L_{\min}/\sigma_s=d$ and followed a similar procedure to decompress the system to $L_{\max}$.

The degree to which the system behaves as hard disks can be estimated using the dimensionless stiffness parameter $\gamma=m_sg/k\sigma_s$, where g is the gravitational acceleration, m_s is the small particle mass, and k is the effective spring constant of the elastic interactions. By measuring the deformation of a plastic (steel) disk under gravity, we estimate $\gamma_{\text{plastic}}\approx1.85\times10^{-3}$ ($\gamma_{\text{steel}}\approx3\times10^{-7}$), which implies that the deviation from hard-disk behavior is small [cf. Figs. 2(a) and 2(d)].

We performed molecular-dynamics (MD) simulations of bidisperse frictionless disks under gravity. Since we are interested in robust features of MS packing probabilities, we do not exactly mimic the packing preparation in experiments. For example, we do not include static frictional forces, but instead use velocity-dependent dissipative forces. However, geometrically similar sets of MS packings are needed to compare the probability distributions. Thus, in simulations and experiments, we closely match the cell geometry, particle size distribution, and gravitational and elastic forces. To enumerate all MS packings and accurately measure their frequencies, we considered small systems from $N=2$ to 7 disks. Systems with an even number of particles contained equal numbers of large and small particles.

We assume that the disks interact via a finite-range, purely repulsive linear spring force

$$\vec{F}^r(r_{ij})=\frac{\varepsilon}{\sigma_{ij}^2}\delta_{ij}\Theta(\delta_{ij})\hat{r}_{ij}, \tag{1}$$

where ε is the elastic energy scale, r_{ij} is the separation between disks i and j, $\sigma_{ij}=(\sigma_i+\sigma_j)/2$ is the average diameter,

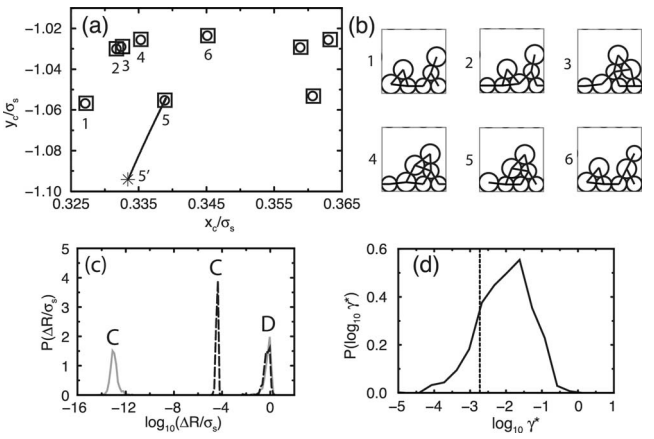

FIG. 2. (a) Coordinates (x_c,y_c) of the centroids of $N=7$ MS packings from experiments (squares) and simulations (circles) for plastic disks. Solid line shows the location of one of the centroids over a range of dimensionless stiffness parameter, $10^{-7}\leq\gamma\leq\gamma^*$, where γ^* (asterisk) is the value at which the MS packing becomes unstable. Along this line, the network of particle contacts remains unchanged. Centroids of six representative configurations are labeled 1 through 6 and the corresponding configurations are shown in (b). Note that two systems with similar x_c and y_c (e.g., packings 2 and 3) can have significantly different contact networks, whereas systems with different x_c and y_c (e.g., packings 5 and 5′) can possess the same contact network. (c) Probability distributions of the separation ΔR in configuration space between distinct MS packings (labeled D) and between a given MS packing and the one furthest away with the same contact network (labeled C) for experiments (dashed lines) and simulations (solid lines). (d) Probability distribution for γ^* from simulations. The vertical line indicates γ_{plastic}.

$\delta_{ij}=\sigma_{ij}-r_{ij}$ is the interparticle overlap, $\hat{r}_{ij}$ is the unit vector connecting particle centers, and $\Theta(x)$ is the Heaviside step function. In simulations at fixed cell width L, where initially randomly placed disks fall under gravity, and quasistatic variation of L using a protocol similar to that for experiments, the system evolves according to Newton's equations of motion

$$m_i\vec{a}_i=-m_ig\hat{y}+\sum_{j\neq i}^{N}[\vec{F}^r(r_{ij})-b\theta(\delta_{ij})\vec{v}_{ij}\cdot\hat{r}_{ij}]\hat{r}_{ij}+F_i^w, \tag{2}$$

where $\vec{a}_i$ is the acceleration of particle i, $\vec{v}_{ij}$ is the relative velocity of particles i and j, and b is the damping parameter. The particle-wall interaction force F^w has an analogous form to the particle-particle interaction with $\varepsilon^w=2\varepsilon$. We set the dimensionless damping parameter to $\bar{b}=\sigma_sb/\sqrt{m_s\varepsilon}=0.25$. At each L, the simulations are terminated when the total force $\vec{F}_{\text{tot}}$ on each particle reaches machine precision.

To determine mechanical stability, we calculated eigenvalues of the dynamical matrix [12]. MS packings possess $2N'$ positive eigenvalues, where $N'=N-N_r$ and N_r is the number of "rattler" disks. Rattlers have fewer than three contacts (including wall contacts). We distinguish MS packings at a given cell width by comparing the eigenvalue lists. The eigenvalues are considered to be equal if they differ by less than the noise threshold 10^{-6}. To compare simulation and

experimental data, we omit rattler particles and consider only particle positions forming the contact network. We find that nearly all MS packings are isostatic with $N_c=2N'$ particle contacts [13].

For each L, we find that MS packings occur as discrete points in configuration space [10]. In Fig. 2(a) we display the centroids $\vec{r}_c=N^{-1}\Sigma_{i=1}^{N}\vec{r}_i$ of MS packings in a region containing several microstates for $N=7$ plastic disks at dimensionless cell width $\lambda\equiv L/\sigma_s=4.253\ 14$. The results show that the centroids are indeed distinct and well separated. Moreover, the experimental and simulation points agree. Our simulations do not involve static frictional forces, thus this agreement indicates that our experimental technique generates frictionless MS packings. In Fig. 2(b), we show the particle configurations that correspond to six of the centroids shown in (a). Note that two systems with similar centroids (e.g., packings 2 and 3) can have significantly different contact networks, whereas systems with different centroids (e.g., packings 5 and 5′) can possess the same contact network. This occurs because we are only visualizing a low-dimensional slice of the $2N$-dimensional configuration space.

Figure 2(c) shows that the scatter in MS packing centroids is several orders of magnitude smaller than the average separation between discrete MS packings in configuration space. The average distance between distinct MS packings is $\approx 0.5\sigma_s$, whereas the maximum size of the scatter is $10^{-12}\sigma_s$ in simulations and $10^{-5}\sigma_s$ in experiments. Thus, in the experimental analysis, two packings are considered to be the same microstate if $\Delta R=|\vec{R}_i-\vec{R}_j|/\sigma_s<10^{-2}$.

To determine if our packings can be treated as hard disks, we tested their stability to changes in the stiffness parameter γ. The solid line in Fig. 2(b) shows the change of position of a MS packing centroid when γ is increased from 10^{-7} to the critical value γ^* where a change in the particle contacts occurs. While the overall change is significant, the position of the centroid for γ_{plastic} is indistinguishable from that in the hard-disk limit $\gamma\to 0$. The distribution of γ^* for the set of all simulation MS packings at wall separation $\lambda=4.253\ 14$ is depicted in Fig. 2(d). These results indicate that most of the hard-disk packings remain stable even when $\gamma > \gamma_{\text{plastic}}$.

In simulations, we perform a large number of trials and find nearly all MS packings in small systems. In Fig. 3(a), we show the number of distinct MS packings N_s versus number of trials N_t for $N=3-7$ at cell width $\lambda=4.253\ 14$. In most cases, we saturate the packing-generation process in the sense that we do not generate new MS packings when N_t is increased by a factor of 10 beyond N_t^{tot}. In experiments, we did not reach saturation due to insufficient number of trials. Figure 3(b) shows that the total number of MS packings grows exponentially with system size [14], $N_s^{\text{tot}}\sim e^{aN}$. The exponent $a\approx 1.2$ is the same as found for periodic systems [10]; however, the prefactor is larger by roughly 1 order of magnitude. The number of trials required to reach saturation of the algorithm [cf., Fig. 3(a)] also grows exponentially with N, but with a larger exponent. As shown in Fig. 3(c) for $\lambda=4.253\ 14$ and Fig. 4 for a range of cell widths λ, MS packing probabilities vary by many orders of magnitude. Figure 3(c) also demonstrates that we find quantitative agreement in the shape of the frequency distributions between simulations and experiments, which implies that MS packing probabilities are weakly sensitive to the dynamics used to generate them.

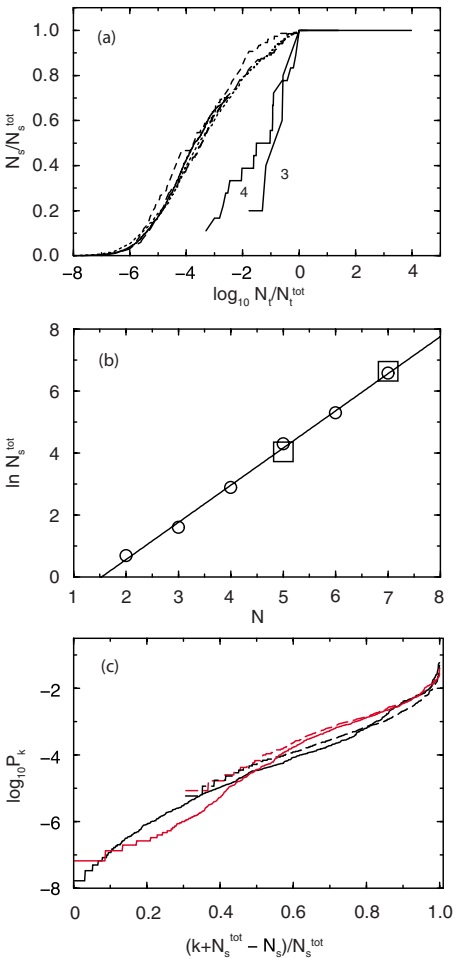

FIG. 3. (Color online) (a) Number of distinct states N_s found in N_t trials for experiments with $N=7$ (solid line) and simulations with $N=3$ (solid, labeled 3), 4 (solid, labeled 4), 5 (dashed), 6 (long dashed), and 7 (dotted) for plastic disks. The horizontal (vertical) axis is scaled by the total number of MS packings N_s^{tot} (trials, N_t^{tot}) at saturation. The experimental curve was obtained by fitting N_s^{tot} and N_t^{tot} to simulations. (b) N_s^{tot} vs N from simulations (circles) and experiments (squares). Solid line has slope 1.2. (c) Sorted probability P_k of MS packings for $N=7$ vs index $(k+N_s^{\text{tot}}-N_s)/N_s^{\text{tot}}$ for simulations (solid black line) and experiments (dashed black line) at cell width $L/\sigma_s=4.253\ 14$. The sorted probability for geometrical family k averaged over all L is also shown for $N=5$ simulations [solid (red) gray line] and experiments [dashed (red) gray line] for steel particles. $N_s/N_s^{\text{tot}}\approx 0.7$ for experiments.

To quantitatively compare MS packings from experiments and simulations, we calculated the distance in configuration space ΔR between each MS packing generated in experiments and the nearest and next-nearest MS packings from simulations. In Fig. 5(a), we show the nearest- and next-nearest-neighbor separations ΔR_n and ΔR_{nn} for $N=7$ steel disks and wall separation $\lambda=4.253\ 14$ versus index k sorted by increasing ΔR_n. For 95% of packings, the nearest- and next-nearest-neighbor distances are well separated, with ΔR_n much smaller than the average distance between distinct MS packings. The separation of length scales in configuration

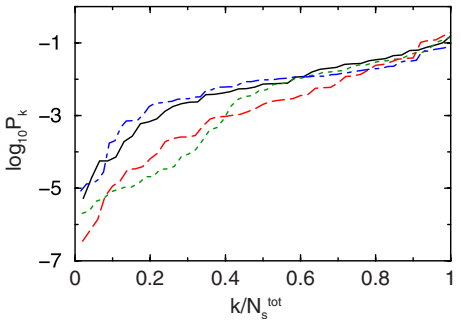

FIG. 4. (Color online) Sorted probability P_k of MS packings for $N=5$ vs index k/N_s^{tot} for simulations of steel particles for four values of the dimensionless wall separation $\lambda=L/\sigma_s=1.5$ (black solid line), 2.4 (red dashed line), 3.6 (blue dot-dashed line), and 4.2 (green dotted line). All curves show strongly nonuniform probabilities.

space allows an unambiguous match between packings from experiments and simulations.

To determine the sensitivity of the probabilities on the packing-generation process, in Fig. 5(b) we compare the probabilities from experiments P_k^{exp} and simulations P_k^{sim} for the *matched* states. We demonstrate a strong correlation between P_k^{exp} and P_k^{sim}: likely packings in experiments tend to

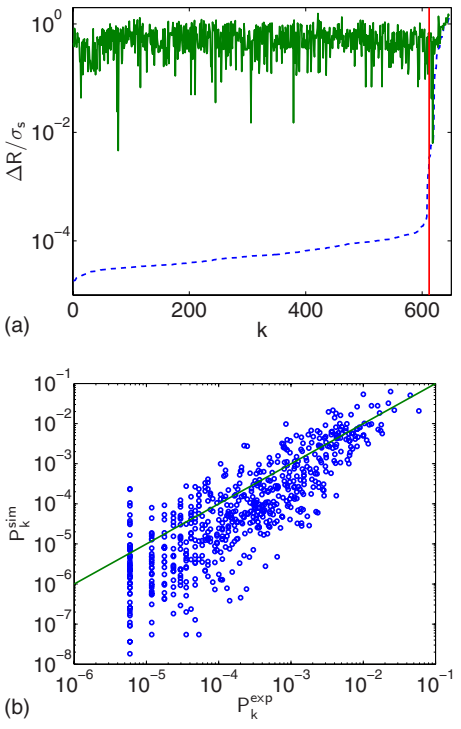

FIG. 5. (Color online) (a) Distances ΔR_n and ΔR_{nn} between each MS packing from experiments and the nearest (blue dotted) and next-nearest (green solid) MS packing from simulations on steel disks vs index k for the experimental MS packings sorted in order of increasing ΔR_n at $\lambda=4.25314$. The vertical line at $k=612$ separates matched and unmatched MS packings. (b) The probability with which MS packings occurred in experiments P_k^{exp} compared to the probability of the matched state in simulations P_k^{sim}. Solid line has slope 1.

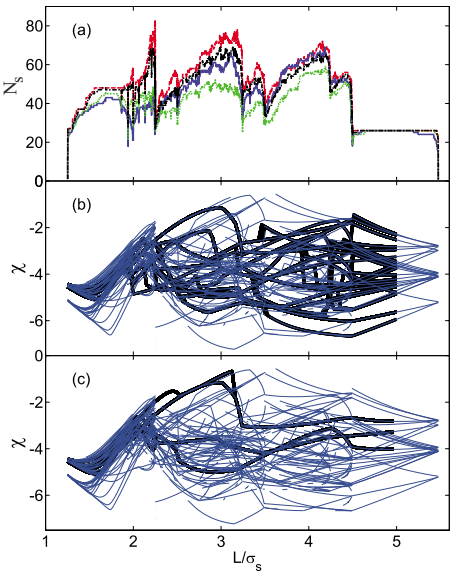

FIG. 6. (Color online) (a) Number of distinct MS packings N_s vs cell width L/σ_s for $N_t=10^5$ (blue) from experiments and 10^5 (green), 10^6 (black), and 10^7 (red) from simulations (from bottom to top at $L/\sigma_s=1.75$) for $N=5$ steel disks. An invariant χ of the distance matrix is plotted vs L/σ_s for experimental packings undergoing quasistatic (b) compression (thick black lines) from $L_{\max}$ to $L_{\min}$ followed by (c) decompression (thick black lines) to $L_{\max}$. In (b) and (c), all MS packings found in simulations are shown as thin blue lines.

be likely in simulations, and rare packings in experiments tend to be rare in simulations (although there is significant scatter). Since the dynamics in experiments and simulations is quite different, this again implies that properties of frictionless MS packings are weakly dependent on the packing-generation protocol.

To investigate whether our results depend strongly on the wall separation L, we generated MS packings in experiments and simulations with randomly selected L from $L_{\min}$ to $L_{\max}$ for $N=5$ steel disks. We assume that MS packings at different L belong to the same geometrical family if they possess the same particle contact network and the family exists at all intermediate L. We tested this assumption by applying quasistatic compression to all families from simulations.

In Fig. 6(a), we show the number of distinct MS packings N_s versus L/σ_s for $N=5$ steel disks and several N_t. The slight oscillating behavior in N_s occurs as layers of particles are added or removed. These results suggest that the experimental and simulation curves will converge to a finite N_s^{tot} upon increasing N_t. We have also verified that at each L, MS packings display highly nonuniform probabilities (cf. Fig. 4). In Figs. 6(b) and 6(c), we relate MS packings at different L by plotting an invariant χ of the distance matrix (the second-largest eigenvalue minus a constant times L) versus L/σ_s, where the entries of the distance matrix give the pair separations between all particles and walls. χ is shown for packings undergoing quasistatic compression [Fig. 6(b)] from $L_{\max}$ to $L_{\min}$ followed by decompression to $L_{\max}$ [Fig. 6(c)] in experiments (thick black lines). In (b) and (c), all MS packings obtained from simulations are also highlighted using

(blue) thin lines. These panels show several remarkable results: (1) MS packings can be classified using a finite number of distinct geometrical families (lines in configuration space) over a continuous range of L; (2) quasistatic evolution leads to strong contraction in the number of sampled MS packings; and (3) transitions from one family to another occur via jumps or kinks in χ. Further, in Fig. 3(c), we show that the probabilities for geometrical families averaged over L are highly nonuniform and have a similar form to that for MS packings at fixed L.

It is important to stress several aspects of our work. First, it is well-known that small *thermal* systems sample phase space with equal probability (e.g., in MD simulations of Lennard-Jones liquids [15]). Thus, it is remarkable that small granular packings occur with highly nonuniform probabilities. Since this nonuniformity increases with system size [11], we expect that highly nonuniform microstate distributions will also occur for macroscopic systems. Second, we believe that studying small systems is an important step in constructing a statistical theory for macroscopic jammed systems. In future investigations, we will quantify the extent to which macroscopic granular systems can be treated as collections of nearly independent small subsystems. Finally, we presented an experimental technique in which we are able to generate and study with exquisite precision the structural and mechanical properties of frictionless packings of granular media.

Financial support from NSF Grants No. CBET-0348175 (G.G., J.B.), No. DMR-0448838 (G.G., C.S.O.), and No. DMS-0835742 (C.S.O.) is acknowledged. We also acknowledge generous amounts of CPU time from Yale's Center for High Performance Computing.

[1] S. Henkes, C. S. O'Hern, and B. Chakraborty, Phys. Rev. Lett. **99**, 038002 (2007).
[2] S. Henkes and B. Chakraborty, Phys. Rev. E **79**, 061301 (2009).
[3] C. Song, P. Wang, and H. A. Makse, Nature (London) **453**, 629 (2008).
[4] M. Pica Ciamarra, A. Coniglio, and M. Nicodemi, Phys. Rev. Lett. **97**, 158001 (2006).
[5] S. F. Edwards and R. B. S. Oakeshott, Physica A **157**, 1080 (1989).
[6] P. Richard, M. Nicodemi, R. Delannay, P. Ribière, and D. Bideau, Nature Mater. **4**, 121 (2005).
[7] H. A. Makse and J. Kurchan, Nature (London) **415**, 614 (2002).
[8] A. Fierro, M. Nicodemi, and A. Coniglio, Phys. Rev. E **66**, 061301 (2002).
[9] A. Barrat, J. Kurchan, V. Loreto, and M. Sellitto, Phys. Rev. Lett. **85**, 5034 (2000).
[10] N. Xu, J. Blawzdziewicz, and C. S. O'Hern, Phys. Rev. E **71**, 061306 (2005).
[11] G.-J. Gao, J. Blawzdziewicz, and C. S. O'Hern, Phys. Rev. E **74**, 061304 (2006).
[12] A. Tanguy, J. P. Wittmer, F. Leonforte, and J.-L. Barrat, Phys. Rev. B **66**, 174205 (2002).
[13] A. V. Tkachenko and T. A. Witten, Phys. Rev. E **60**, 687 (1999).
[14] F. H. Stillinger, J. Chem. Phys. **88**, 7818 (1988).
[15] D. Thirumalai, R. D. Mountain, and T. R. Kirkpatrick, Phys. Rev. A **39**, 3563 (1989).